M. Bazrafshan
Materials innovation institute (M2i),
van der Burghweg 1,
Delft 2628 CS, The Netherlands;
Laboratory for Surface Technology and Tribology,
Department of Engineering Technology,
University of Twente,
P.O. Box 217,
Enschede 7500AE, The Netherlands
e-mail: m.bazrafshanfadafan@utwente.nl

M. B. de Rooij
Laboratory for Surface Technology and Tribology,
Department of Engineering Technology,
University of Twente,
P.O. Box 217,
Enschede 7500AE, The Netherlands
e-mail: m.b.derooij@utwente.nl

E. G. de Vries
Laboratory for Surface Technology and Tribology,
Department of Engineering Technology,
University of Twente,
P.O. Box 217,
Enschede 7500AE, The Netherlands
e-mail: e.g.devries@utwente.nl

D. J. Schipper
Laboratory for Surface Technology and Tribology,
Department of Engineering Technology,
University of Twente,
P.O. Box 217,
Enschede 7500AE, The Netherlands
e-mail: d.j.schipper@utwente.nl

Evaluation of Pre-Sliding Behavior at a Rough Interface: Modeling and Experiment

One of the main issues in precision engineering is the lack of deep understanding of the pre-sliding behavior at the interface of mating surfaces of positioning mechanisms. In addition to the mechanical properties of the contacting bodies, their surface topography plays a key role in the pre-sliding regime and has a great impact on the frictional stiffness. This paper experimentally evaluates a boundary element method (BEM) model for the pre-sliding behavior at the interface of a smooth silicon wafer and a rough polymeric ball. The polymeric ball is either high-density polyethylene (HDPE) or polyoxymethylene (POM). The experiments are conducted at three different normal loads on five different spots on the wafer. The sliding stroke and coefficient of friction are extracted from experiments to be implemented as inputs to the numerical model. The roughness of the balls is also another input. The numerical and experimental friction hysteresis loops are compared. There is a small difference in the predicted pre-sliding distance from the experiments. The lateral stiffness, calculated at three different points on the pre-sliding regime of friction hysteresis loops, is compared with the Mindlin's solution and experimental values for both contact interfaces and normal loads. [DOI: 10.1115/1.4045900]

Keywords: pre-sliding, lateral stiffness, roughness, boundary element method, experiment, simulation, computational mechanics

1 Introduction

Achieving high-precision positioning is one of the main goals in precision engineering. Nevertheless, the friction between the mating surfaces of the sliding components of the mechatronic devices gives rise to a positioning inaccuracy. Friction is commonly divided into two regimes of partial slip and full slip. As the former one is treated as a more crucial phenomenon due to the complexity of stick to slip transition, its understanding and prediction are vital for more accurate positioning.

Initial studies on the partial slip contact have been conducted independently by Cattaneo [1] and Mindlin [2] for the elastic contact at the smooth interface of a ball and a flat, where, within the circular contact area, a central sticking zone is surrounded by an annulus of slip which develops toward the center of contact upon an increase in the tangential force and finally covers the entire contact area and starts the full slip state as soon as the tangential force reaches the static friction force. Later on, Mindlin and Deresiewicz extended this solution to deal with an oscillating tangential force, which leads to friction hysteresis behavior [3].

In the original Mindlin solution, it was assumed that the contacting materials are identical. This assumption simplifies the solution since the normal pressure and shear stress components become decoupled and cannot affect each other as they cannot induce any deformations in the other directions. The contact of dissimilar materials, nevertheless, does not follow this condition, and the normal pressure and shear stress components are coupled. Since there is no analytical solution for this complex problem, researchers have resorted to numerical solutions such as finite element method (FEM) [4–6] and boundary element method (BEM) [7–11].

All these analytical and numerical approaches deal with contact at a smooth interface. In reality, however, engineering surfaces have a certain level of roughness, meaning that the microgeometry details of the mating surfaces at the asperity level determine how the surfaces interact. The mentioned approaches form the basis for multi-asperity methods where the single-asperity solutions are combined with a statistical distribution of asperities, such as Gaussian, to study the partial slip and full slip friction [12–17]. Experiments have also been conducted to evaluate the roughness effect on the pre-sliding behavior and possibly compare the results with those of such models. Al-Bender and Moerlooze combine the Maxwell-Slip model with the Greenwood-Williamson theory for the contact of rough surfaces to evaluate the experimental relation between the normal load and the friction force in the pre-sliding regime [18,19]. Eriten et al. investigated the impact of roughness on the frictional energy dissipation in the fretting contact between two nominally flat rough surfaces by considering the probability distribution of asperities [20]. They quantitatively showed that rougher surfaces dissipate more energy. Song and Yan conducted experiments to relate the friction and normal forces with the real contact area, measured optically at the interface of two transparent polymethyl methacrylate blocks [21]. Raeymaekers and Talke studied the effect of laser polishing on the fretting wear behavior at the interface between a rough hemisphere and a flat plate [22]. They did not observe any noticeable difference in the wear production between a laser polished and a regular stainless steel hemisphere.

Contributed by the Applied Mechanics Division of ASME for publication in the Journal of Applied Mechanics. Manuscript received September 27, 2019; final manuscript received December 29, 2019; published online January 8, 2020. Assoc. Editor: Yong Zhu.

Researchers have also pursued other numerical methods due to the well-known limitations of multi-asperity methods such as the lack of interaction between asperities. Pohrt and Li [23] and Paggi et al. [24] proposed a conjugate gradient method -based BEM model for the partial slip contact at a rough interface. They assumed a unidirectional shear stress proportional to the normal pressure in the slip zone. Yet, they did not take the coupling between the normal pressure and shear stress into account. Grzemba et al. proposed a characteristic length parameter defining the crossover from sticking to slipping for the contact of self-affine fractal surfaces [25]. Kasarekar et al. developed a numerical approach to study the fretting wear under partial slip conditions [26]. They found the roughness details at small length-scales a major factor in wear simulations. Chen et al. extended their previously developed BEM model for the point contact of dissimilar materials to evaluate the static friction force and coefficient of friction at a rough interface of a ball and a flat [27]. They set a constant shear strength all over the contact area as a local criterion for the transition from stick to slip.

Although there seems to be rich literature on the pre-sliding behavior at a rough interface of two contacting surfaces, the experimental evaluation of a numerical model while using the measured topography of the contacting surfaces and taking the coupling between the normal pressure and the contact shear stress components into account is scarce. Therefore, the aim of this paper is to experimentally evaluate the recently developed BEM model for the stick-slip transition at a rough interface [28]. First, a summary of the proposed BEM model for the hysteresis behavior of the friction at a rough interface is provided. In Sec. 3, the test setup is explained. Section 4 deals with the simulation using the input data to be compared with experimental results in Sec. 5. Finally, the conclusion is provided in Sec. 6.

2 Boundary Element Method Model

This section summarizes a recently proposed BEM model for the hysteresis behavior of the adhesive friction at the rough interfaces of two contacting bodies [28]. As the adhesion can be neglected due to the relatively rough (large local slopes) interface of the polymeric ball, the same numerical methodology, excluding the adhesion part, is implemented in this study. Figure 1 illustrates the contact of two bodies in the xz plane, where it is loaded with the constant normal force of F_0 and the tangential force of F_x. The resulted contact pressure and shear stress components in x and y directions are represented by $p(x, y)$, $q_x(x, y)$, and $q_y(x, y)$, respectively. The deformation, rigid body displacement, and relative displacement in the x-direction (y-direction) are also denoted by u_x, δ_x, and $s_x(u_x, \delta_x, s_y)$, respectively, where

$$\begin{cases} s_x(x, y) = u_x(x, y) - \delta_x \\ s_y(x, y) = u_y(x, y) - \delta_y \\ g(x, y) = u_z(x, y) + h(x, y) - \delta_z \end{cases} \tag{1}$$

Here, $h(x, y)$, $g(x, y)$, $u_z(x, y)$, and δ_z are initial and final separation profiles, deformation and rigid body displacement (indentation or approach) in the z-direction, respectively. It is noted that the initial separation profile (the separation right before the contact forms) is determined by the roughness height profiles of the contacting surfaces, $z_1(x, y)$ and $z_2(x, y)$. In other words

$$h = \max(z_1) + \max(z_2) - (z_1 + z_2) \tag{2}$$

Depending on the friction force, the contact can experience either of the two states of the partial slip or full slip. As long as the friction force is smaller than the static friction force (the force required for the start of full slip), the contact area is sticking in some regions and slipping in the rest, though there is no macroscopic relative displacement between the two contacting surfaces. As soon as the friction force reaches the static friction force, the entire contact area experiences the slip state, and therefore, the full slip or gross sliding starts. In this state, the two surfaces move macroscopically with respect to one another. For a quasi-static tangential loading, where the friction force is history-dependent, there are two criteria to distinguish between stick and slip regions within the contact area. In the stick regime, the shear stress is smaller than friction coefficient times the local pressure and the rate of relative displacement is zero. In the slip region, however, the shear stress is equal to the friction coefficient times local pressure and the rate relative displacement is no longer zero. These criteria are mathematically given by

$$\begin{aligned} A_{st} &= (x, y) \in A_c \left| \sqrt{q_x(x, y)^2 + q_y(x, y)^2} < \mu_f p(x, y), \right. \\ &\quad \sqrt{\Delta s_x(x, y)^2 + \Delta s_y(x, y)^2} = 0 \\ A_{sl} &= (x, y) \in A_c \left| \sqrt{q_x(x, y)^2 + q_y(x, y)^2} = \mu_f p(x, y), \right. \\ &\quad \sqrt{\Delta s_x(x, y)^2 + \Delta s_y(x, y)^2} \neq 0 \end{aligned} \tag{3}$$

Here, Δ refers to the change of a parameter between two consecutive loading steps.

Given the contact geometry (roughness height profiles of the contacting surfaces) and elastic properties of the materials, normal force, friction coefficient, and tangential loading path, the BEM model first solves the normal contact problem to find the contact pressure and separation profiles, while meeting the complementarity conditions given as

$$\begin{aligned} &p(x, y) = 0, \quad \text{at } g(x, y) > 0 \\ &p(x, y) > 0, \quad \text{at } g(x, y) = 0 \\ &\int_\Omega p(x, y)\, dx\, dy = F_0 \end{aligned} \tag{4}$$

which states that the pressure is zero at separated areas (where $g > 0$), while it is positive at contact areas (where $g = 0$). Moreover, the summation of the pressure over the contact problem domain, Ω, must be the same as the external normal force for the static equilibrium of the system.

The next step is to find the shear stress components at each loading step meeting the criteria given in Eq. (3). It is very important to note that the effect of shear stress components on the contact pressure is also included in an iterative manner. More details on the numerical procedure to solve this problem can be found in Refs. [28–30].

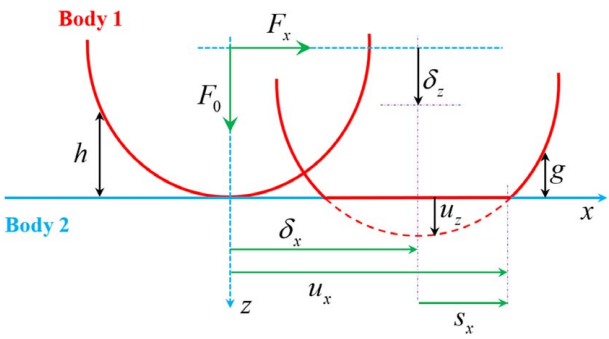

Fig. 1 Contact variables

3 Experiments

The experimental setup, as shown in Fig. 2, consists of three positioning stages and three capacitive sensors. The Z- and XY-positioning stages have a stroke of 18, 26, and 18 mm, and resolutions of 20 nm, 0.2 nm, and 100 nm, respectively. The elastic hinge behind the indenter acts as the force measuring mechanism

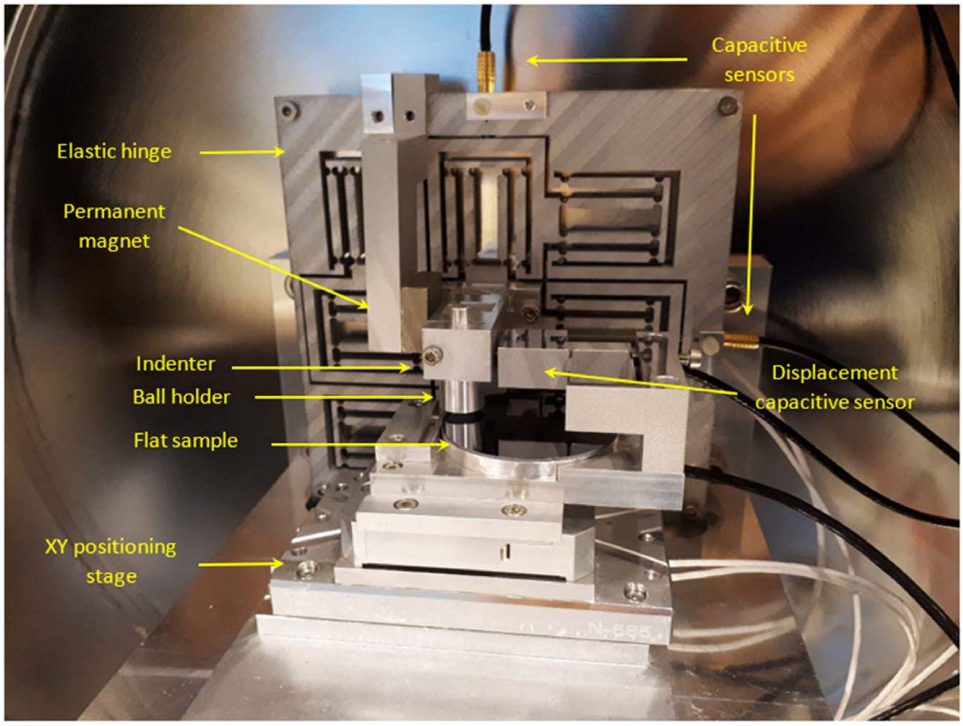

Fig. 2 Experimental test rig

of the setup with two-degrees-of-freedom to measure normal and tangential forces as independently as possible (the reader is referred to [31] for more details about this mechanism).

The setup has a ball-on-flat configuration, where the polymeric ball, with 10 mm of diameter, is fixed inside the ball holder. The ball holder is mounted on the indenter, which is centrally fixed at the elastic hinge, which in turn mounted, along with a back plate, on the Z stage which is placed behind the back plate (not visible in Fig. 2). This stage is used to bring the ball into contact with the flat surface, placed on the XY-stage, and apply the normal load up to 100 mN with an accuracy of 8 μN. To apply the tangential load thereafter, the X-stage moves reciprocally in the X-direction. The Y-stage is used to conduct parallel measurements on the flat surface. In addition, a permanent magnet, as an eddy current damper, is placed close to the indenter to reduce the vibration induced by the Z-positioning stage.

Two of the capacitive sensors, with the resolution of <0.15 nm and measuring range up to 50 μm, are mounted on the elastic hinge. Having the elastic hinge calibrated for its stiffness in Z- and X-directions, the recorded deflections by these two sensors are used to measure the normal and friction forces. The third similar capacitive sensor, with the ultrahigh resolution of better than 0.2 nm and measuring range up to 50 μm, is mounted on the XY-stage to measure the true contact displacement and exclude the deformations of the elastic hinge and the indenter. It must be noted that since this sensor does not see the displacement due to the bending of the ball holder and neither due to the torsion of the elastic hinge and the indenter, an FEM simulation has been carried out to ensure that this displacement is negligible in comparison with the measured tangential displacements.

Before the measurements, the samples are rinsed with isopropanol alcohol and then dried with nitrogen to remove any possible dirt particles from the samples. The entire setup is also placed in a chamber, which is kept closed during the measurements. The temperature and relative humidity of the environment are 22 °C and 35%, respectively.

Both normal and tangential loadings are conducted in a quasi-static manner. First, the Z-positioning stage moves downward at the speed of 1 μm/ sec to reach the desired normal force after the contact is made. Then, having the normal load fixed, the XY-stage moves reciprocally, for a given number of cycles and sliding stroke, in X-direction at the speed of 0.1 μm/ sec. For either of the high-density polyethylene (HDPE) or POM (polyoxymethylene) balls in contact with the silicon wafer, the friction tests are conducted at five different spots and three normal loads for each spot.

Figure 3(*a*) depicts a typical friction force measurement with the setup, shown in Fig. 2, for a normal load of 75 mN and a sliding stroke of 9 μm applied by the X-stage, where the horizontal axis is the displacement recorded by the displacement capacitive sensor. The asymmetry of the hysteresis loop with respect to the vertical axis is due to two reasons. One is the asymmetry of the displacement path itself, which varies between zero and the given sliding stroke. The other reason can be explained by Fig. 3(*b*), which provides a schematic representation of the friction force measurement mechanism. Here, the ball is in contact with the silicon wafer, clamped on the XY-stage, through a spring-slider contact element. The spring constant of this element K_c denotes the contact stiffness and the slider, similar to the Coulomb friction model, has a certain threshold of force (static friction force) and has no relative displacement with respect to the wafer as long as the friction force is below this threshold. The contact element is in series with another spring, K_s, denoting the setup stiffness. The frame O is attached to the ground and x_{ps} denotes the displacement of the XY-stage. Moreover, the frame O′ is attached to the XY-stage and x_{cs}, as measured by the displacement capacitive sensor, represents the absolute displacement of the ball with respect to the wafer (it excludes the setup deformation from the stage displacement). Therefore, x_{ps}, as an input to the experiments, must always be larger than x_{cs} and the measured friction loop is asymmetric with respect to the vertical axis.

The point to note here is that the curved corner of the hysteresis loop at the end of each stroke is due to the visco-elasticity of the polymeric ball which tends to move even after the sliding direction has reversed. This phenomenon can be alleviated by decreasing the sliding speed as much as possible. In fact, in the current experiments which are carried out at the lowest possible speed of the XY-stage (0.1 μm/sec), this effect is already minimized.

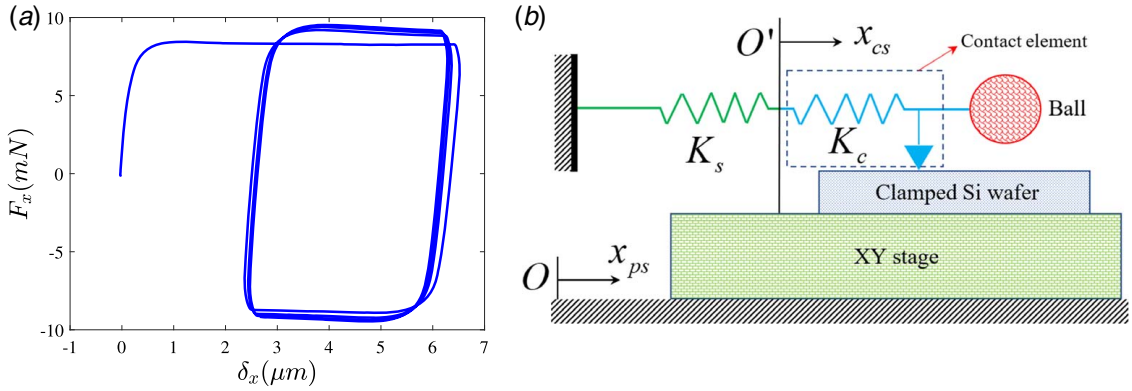

Fig. 3 (*a*) Typical friction force measurement with 75 mN of normal force and 9 μm as the sliding distance of the XY-positioning stage and (*b*) schematic representation of the friction force measurement

4 Simulation

The first step to numerically predict the friction hysteresis loops, to be compared with experimental ones, is to measure the roughness of the contacting surfaces. The roughness of the polymeric balls after the final friction measurements is measured using a Sensofar confocal microscope (50× magnification). The 1.1 mm × 1.1 mm measured images of the HDPE and POM balls, with 1024 pixels in each direction, are shown in Fig. 4 with a zoomed-in view to see the highest asperities where the contact patches form. The flattened roughness height of the balls (by removing its spherical background) is also depicted in Fig. 5. The RMS roughness values suggest that the HDPE ball has a rougher surface than the POM.

In the current study, the contact pressures are low enough to neglect any possible plastic deformation of the ball during the friction measurements. Even if there were any, they could be easily neglected for the final measurements (that are presented here) as they have happened during the initial measurements. The silicon wafer is also so smooth that its roughness can be neglected in comparison with that of the polymeric balls. Therefore, the flat surface is assumed to be ideally smooth. Two of the inputs to the numerical model are extracted from the experimental results. First is the stroke and second the coefficient of friction.

The stroke d_s is the range of tangential displacement measured by the third capacitive sensor. For this, only the last loop of the friction hysteresis, which is the converged (most stable) one, for each measurement is selected, and then, the stroke is considered to be in the range between the minimum and maximum displacement on this loop. As the measurements are carried out on five different spots, the average of the stroke for each point (at each normal load), as

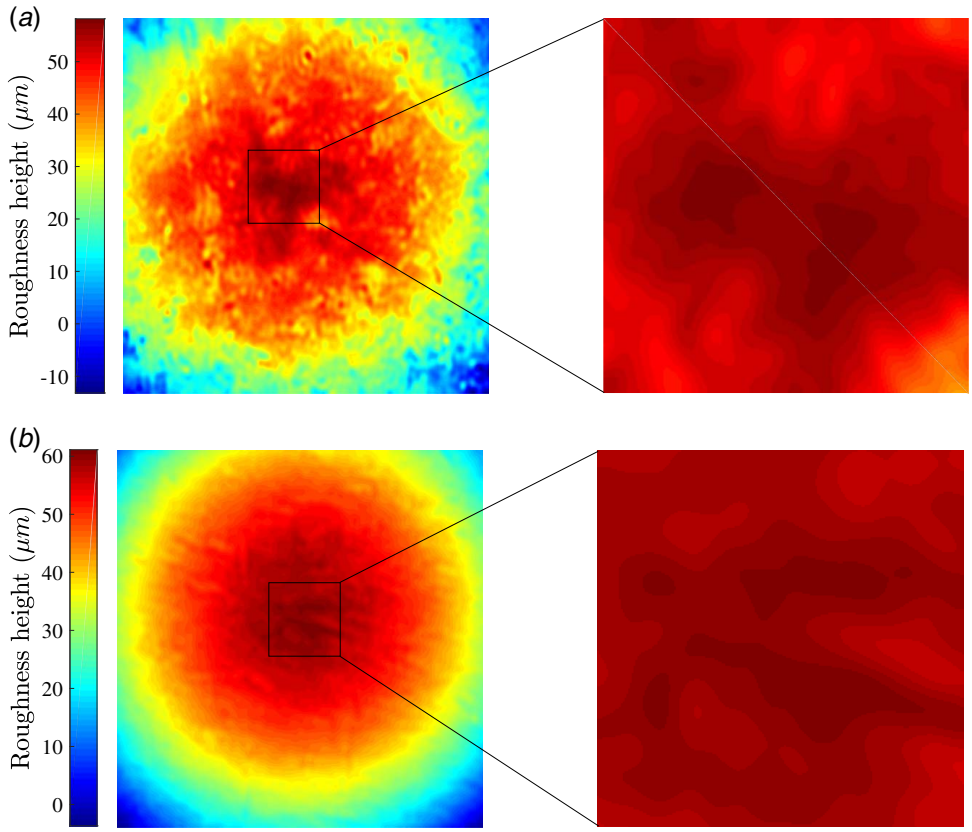

Fig. 4 Roughness height of the balls (1.1 mm × 1.1 mm area in the left and the 0.2 mm × 0.2 mm zoomed-in view in the right): (*a*) HDPE and (*b*) POM, the ball diameter is 10 mm

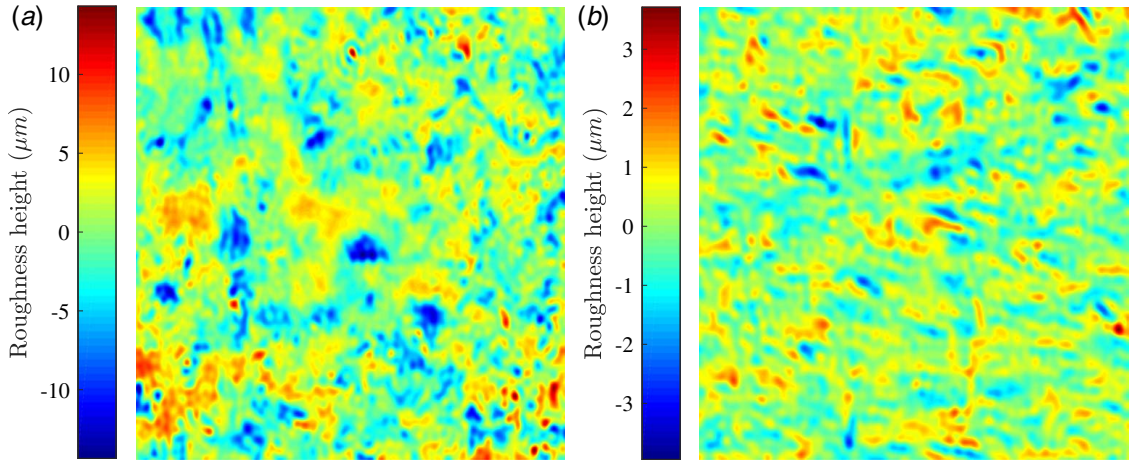

Fig. 5 Flattened roughness height of the (*a*) HDPE and (*b*) POM balls (on a 1.1 mm × 1.1 mm area)

Table 1 Average values of stroke and friction coefficient, extracted from experimental results, used as inputs to the numerical simulation

	d_s (μm)		μ_f	
F_0 (mN)	HDPE	POM	HDPE	POM
25	2.805	2.700	0.153	0.108
50	2.943	3.370	0.146	0.104
75	3.697	4.264	0.129	0.099

given in Table 1, is used as one of the mentioned experimental inputs to the simulation. Therefore, rather than a loading path, a displacement path (of four cycles), as shown in Fig. 6, is considered to be the input to the simulation, similar to the experiments. As the friction takes a few loops to converge, due to the dissimilarity of the contacting surfaces (see [7,8]), only the last loop of the simulation (the converged one) is considered to be compared with experiments.

The coefficient of friction is also calculated as the ratio of the sliding friction force to the normal force. For each set of normal load, the stroke and friction coefficient are extracted separately. The average value of this parameter is also listed in Table 1.

The elastic moduli of HDPE and POM balls have been measured using an Anton Paar nanoindentation tester (NHT^2). For each ball, the measurements are conducted on 25 spots of a 1000 times polished cross-section. Figure 7 shows one of the load–indentation curves for the HDPE ball. The indentation load used is 10 mN with a (un)loading rate of 20 mN/min and a holding time of 60 s. The Berkovich tip used for indentation is calibrated using a pulse-echo calibrated fused silica sample. Measurement results

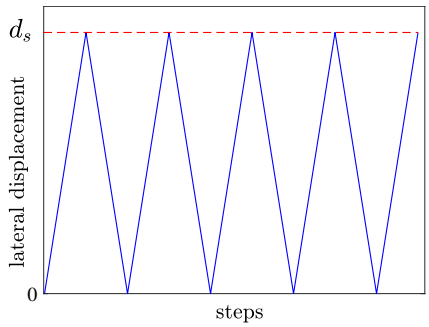

Fig. 6 Displacement path

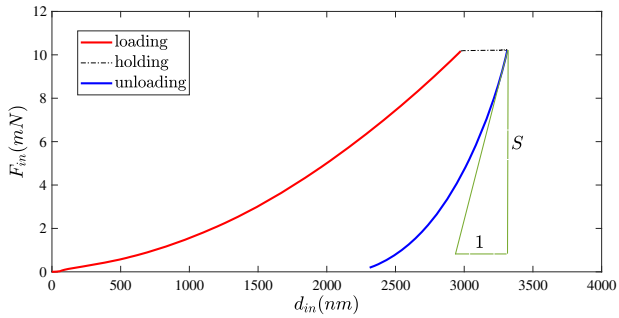

Fig. 7 Load–indentation curve for one spot on the HDPE ball, measured by the nanoindentation tester

were fitted using Oliver and Pharr [32] in combination with a viscous correction obtained by the hold curve at maximum load [33]. The apparent contact stiffness ($S = dF_{in}/dd_{in}$ in Fig. 7) at the onset of unloading is used to define the reduced modulus (E_r). Due to viscous effects, the modulus would be overrated and therefore can be corrected by fitting the holding curve at maximum load. The corrected stiffness S_e can be calculated from the apparent stiffness by

$$\frac{1}{S_e} = \frac{1}{S} + \frac{\dot{d}_{in}}{\dot{F}_{in}} \tag{5}$$

where $\dot{d}_{in}$ and $\dot{F}_{in}$ are the displacement rate at the onset of unloading and the unloading rate, respectively. The reduced modulus therefore would be

$$E_r = \frac{\sqrt{\pi}}{2} \times \frac{S_e}{\sqrt{A_c}} \tag{6}$$

and

$$d_c = d_{in}^{\max} - \varepsilon \frac{F_{in}^{\max}}{S_e} \tag{7}$$

where the indentation depth d_c is used to calculate the area A_c at maximum load $F_{\max}$ using a geometric constant $\varepsilon = 0.75$. With the indenter properties as $E_{diamond} = 1141$ GPa and $\nu_{diamond} = 0.07$ and also $\nu_{polymer} = 0.5$, the material elastic modulus $E_{polymer}$ is calculated using

$$\frac{1-\nu_{polymer}^2}{E_{polymer}} = \frac{1}{E_r} - \frac{1-\nu_{diamond}^2}{E_{diamond}} \tag{8}$$

Table 2 Mechanical properties of the contacting surfaces

	Silicon wafer	HDPE	POM
Elastic modulus (GPa)	130	0.98	1.38
Poisson's ratio	0.28	0.50	0.50
Roughness RMS (μm)	$\simeq$0	3.17	0.67

In the end, the average values as well as the elastic properties of the silicon wafer (as provided by the supplier) are listed in Table 2.

5 Results and Discussion

Given the surface topography and mechanical properties of the contacting surfaces along with the loading conditions, the simulation has been conducted to predict the frictional behavior at the contact of either of the balls against a silicon wafer. Figures 8 and 9 show the contact pressure at the interface of HDPE with POM balls against the wafer, respectively, at three different normal loads. As can be seen, only a small central part of the balls with rather higher heights (see Fig. 4) touches the counter surface. It should be also noted that the calculated contact pressures are small enough to neglect any plastic deformation of the balls.

In the pre-sliding regime of the frictional contact, three points of A, B, and C, as shown in Fig. 10, are chosen to evaluate the partial slip behavior. The normalized shear stress $\sqrt{q_x^2+q_y^2}/\mu_f p$ is used to demonstrate the development of the slip zone (and the shrinking of stick zone) in the contact area. Based on the definition of Eq. (3), this parameter is smaller than and equal to unity in the stick and slip regions, respectively. The development of the slip region on the contact area for both studied contact interfaces at the mentioned three normal loads is shown in Figs. 11 and 12. It is noted that the contact area is a combination of stick and slip regions. Going from points A to C, the imposed tangential displacement increases both local relative displacements and shear stress so that some previously sticking regions enter the slipping regime. This behavior will continue until the slip region covers the entire contact area and the sticking region completely disappears (point D). At this moment, the gross sliding or full slip regime starts and continues until the direction of imposed displacement is reversed (point E).

Figures 13 and 14 compare the experimental and numerically predicted friction hysteresis loops for both HDPE and POM contacts against a silicon wafer, measured at five different spots, while using the stroke and friction coefficients extracted from these experiments (given in Table 1).

In fact, the rhomboids of simulation and measurements match in their width and height since the coefficient of friction and the stroke

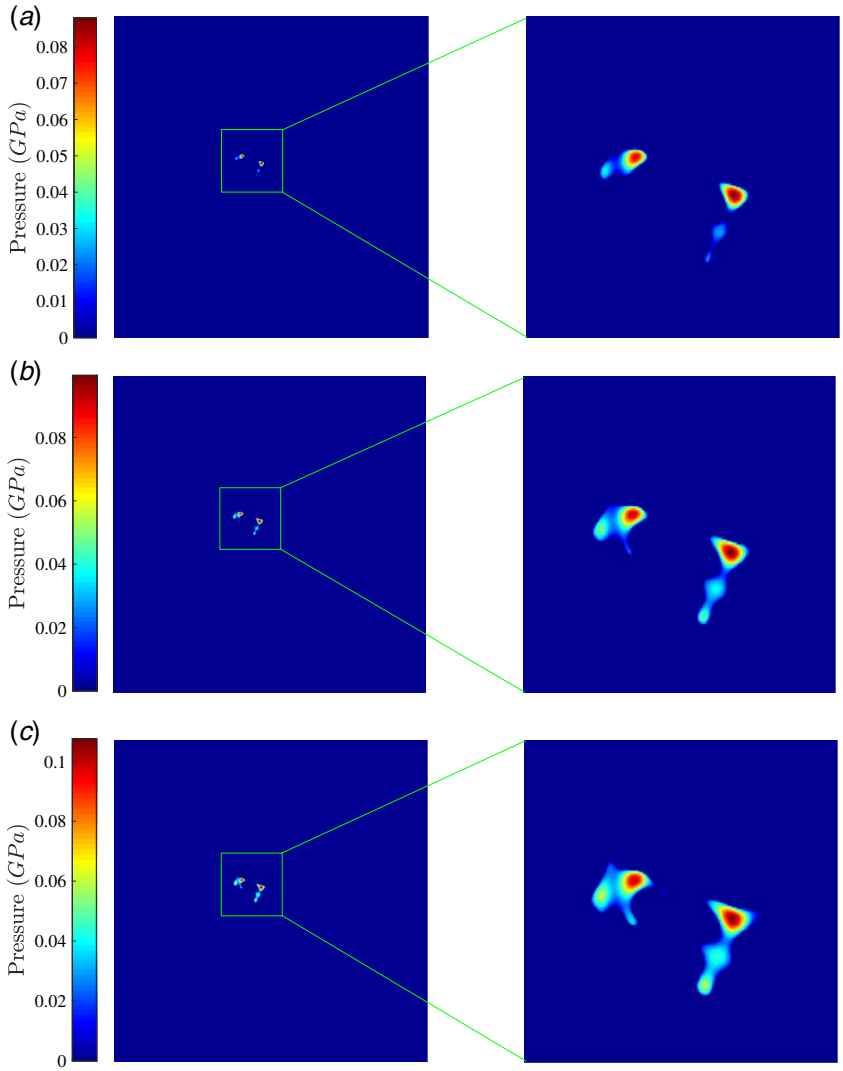

Fig. 8 Contact pressure at the HDPE ball–silicon wafer interface, the 1.1 mm × 1.1 mm area (left) and the 0.2 mm × 0.2 mm zoomed-in view (right): (*a*) $F_0 = 25$ mN, (*b*) $F_0 = 50$ mN, and (*c*) $F_0 = 75$ mN

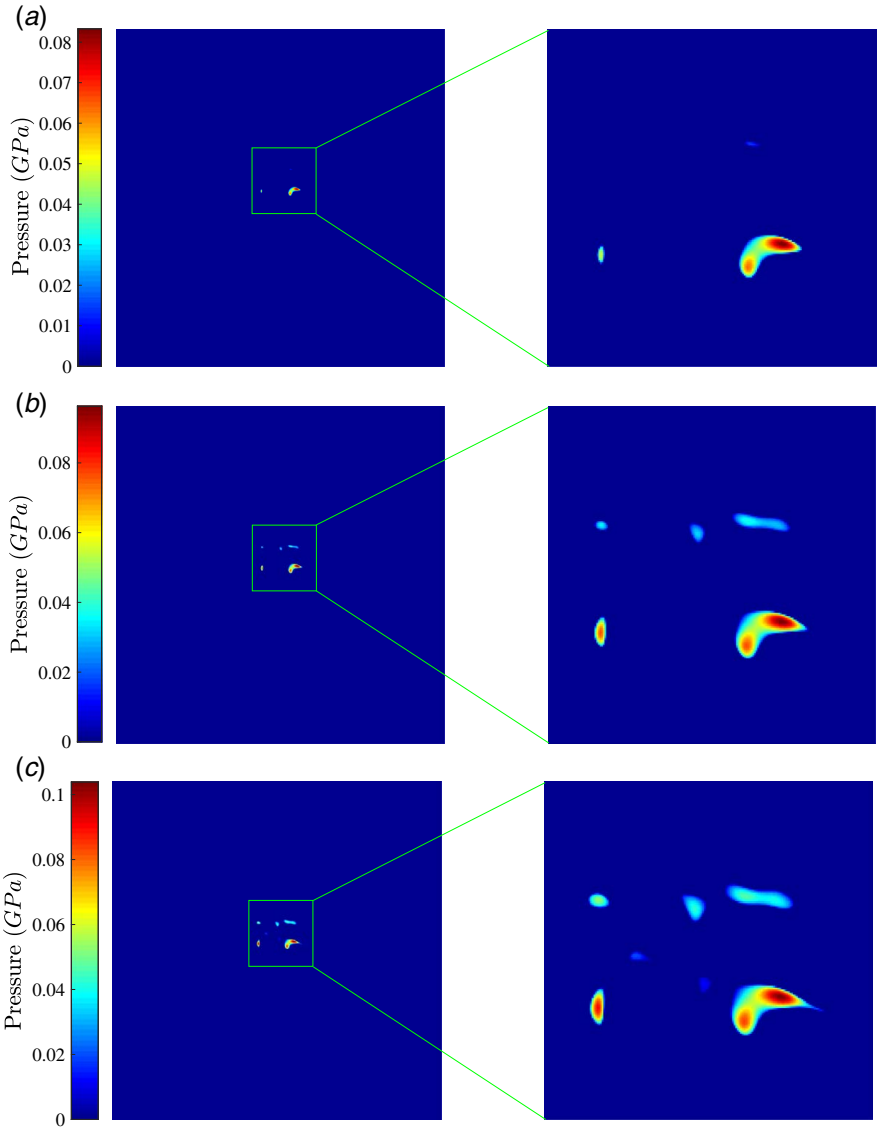

Fig. 9 Contact pressure at the POM ball–silicon wafer interface, the 1.1 mm × 1.1 mm area (left) and the 0.2 mm × 0.2 mm zoomed-in view (right): (*a*) $F_0 = 25$ mN, (*b*) $F_0 = 50$ mN, and (*c*) $F_0 = 75$ mN

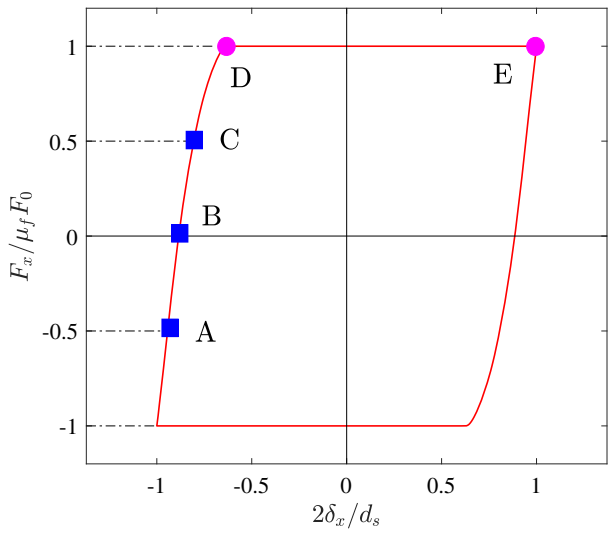

Fig. 10 Position of selected spots on friction hysteresis loop

are set equal. The only thing that can be compared is the run of the curve in the vertical sections or namely the pre-sliding regime, in particular, the angle of these sections. This leaves us with only the incremental stiffness to be compared. Therefore, to have a quantitative comparison between experiments and simulations, the lateral stiffness of the contact K_L defined as the slope of the friction hysteresis loop in the pre-sliding regime is evaluated at points A, B, and C both numerically and experimentally. To calculate the slope more accurately, rather than a finite difference approach, a curve with the form of $F_x = c_1(1-(1-c_2\delta_x)^n)$ (by analogy to the Mindlin solution) is fitted on the pre-sliding region of the friction hysteresis loop in order to calculate the lateral stiffness analytically as

$$K_L(\delta_x) = \frac{dF_x}{d\delta_x} = c_1 c_2 n(1-c_2\delta_x)^{n-1} \tag{9}$$

Here, c_1, c_2, and n are the fitting parameters to be calculated for each fit separately.

Based on the Mindlin solution for the frictional contact between a smooth ball and a flat, the friction force versus tangential lateral

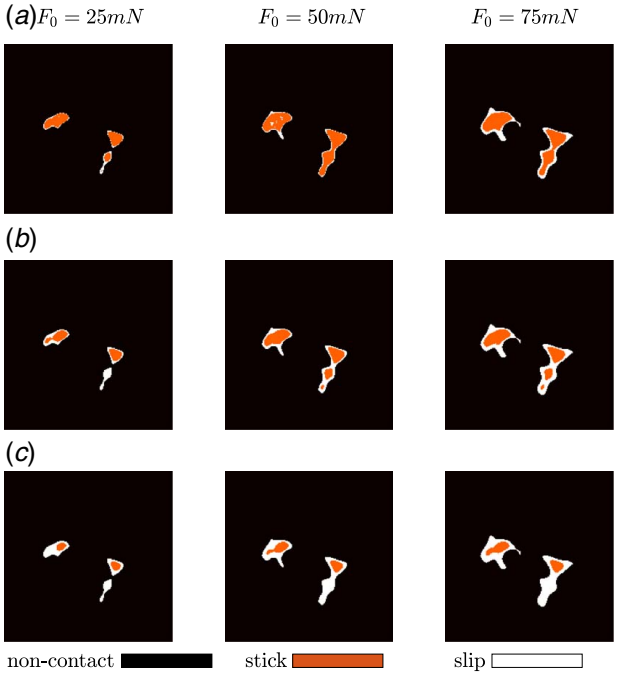

Fig. 11 Stick-slip transition from points A to C (see Fig. 8) for three different normal loads: HDPE ball–silicon wafer contact (on the 0.2 mm × 0.2 mm zoomed-in view).

displacement is expressed by

$$F_x = \mu_f F_0 \left(1 - \left(1 - \frac{\delta_x}{\delta_0}\right)^{3/2}\right), \quad \delta_0 = \frac{3\mu_f F_0}{16 a G_s} \tag{10}$$

here $1/G_s = (2-\nu_1)(1+\nu_1)/2E_1 + (2-\nu_2)(1+\nu_2)/2E_2$, where $E_{1,2}$ and $\nu_{1,2}$ are the elastic modulus and Poisson's ratio of the contacting

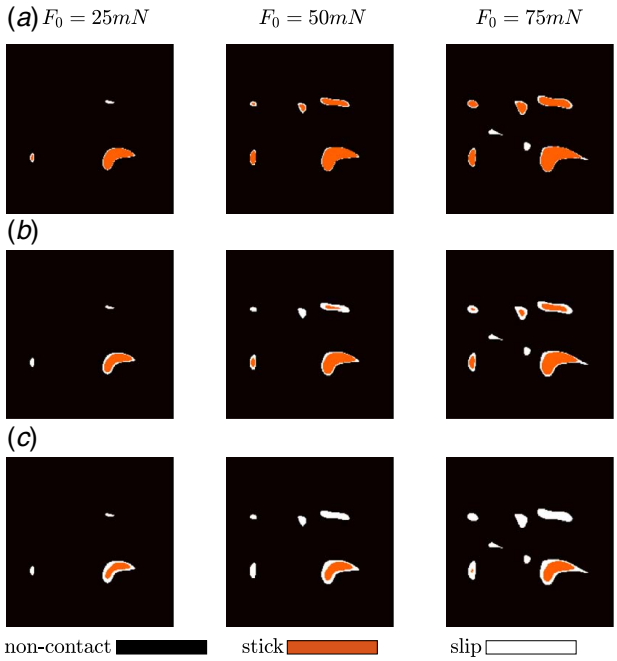

Fig. 12 Stick-slip transition from points A to C (see Fig. 9) for three different normal loads: POM ball–silicon wafer contact (on the 0.2 mm × 0.2 mm zoomed-in view).

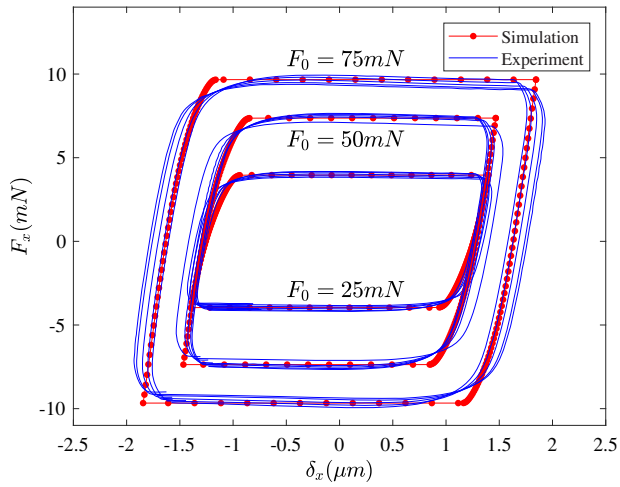

Fig. 13 Comparison between simulation and experimental friction hysteresis loops for HDPE ball–silicon wafer contact

materials. The Hertzian contact radius a is also given by

$$a^3 = \frac{3F_0 R}{4E_s} \tag{11}$$

where R is the ball radius and $1/E_s = (1-\nu_1^2)/E_1 + (1-\nu_2^2)/E_2$. Equation (10) gives rise to the Mindlin's lateral stiffness as

$$K_L^{Mindlin} = \frac{3\mu_f F_0}{2\delta_0}\left(1 - \frac{\delta_x}{\delta_0}\right)^{1/2} = 8aG_s\left(1 - \frac{F_x}{\mu_f F_0}\right)^{1/3} \tag{12}$$

Figure 15(*a*) and 15(*b*) compares the lateral stiffness values at points A, B, and C for the three normal loads at the interface of HDPE and POM balls against the silicon wafer, respectively, between experimental and numerical results and Mindlin's solution. The experiments are quite stable in terms of the lateral stiffness as the spread in this parameter for each case is rather narrow. The largest discrepancies between simulation and experiments are observed at point A which is closer to the left corner of the vertical part of the hysteresis loops and, therefore, more sensitive to the experimental curvy corners. It is confirmed that from point A to point C, the lateral stiffness decreases as a larger part of the contact area is slipping and experiencing a greater relative displacement, and thus, the contact becomes laterally more compliant.

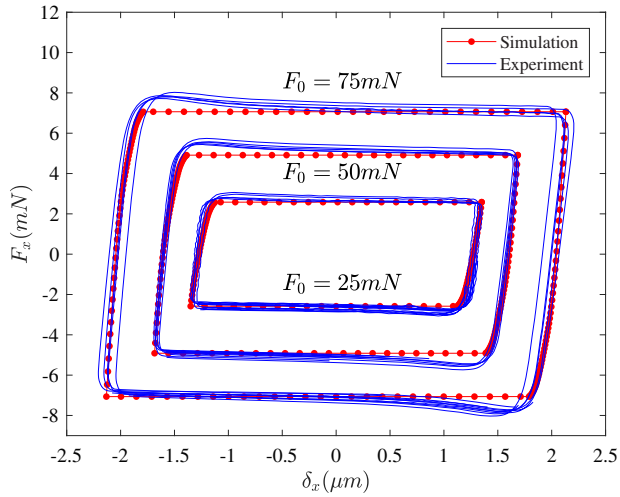

Fig. 14 Comparison between simulation and experimental friction hysteresis loops for POM ball–silicon wafer contact

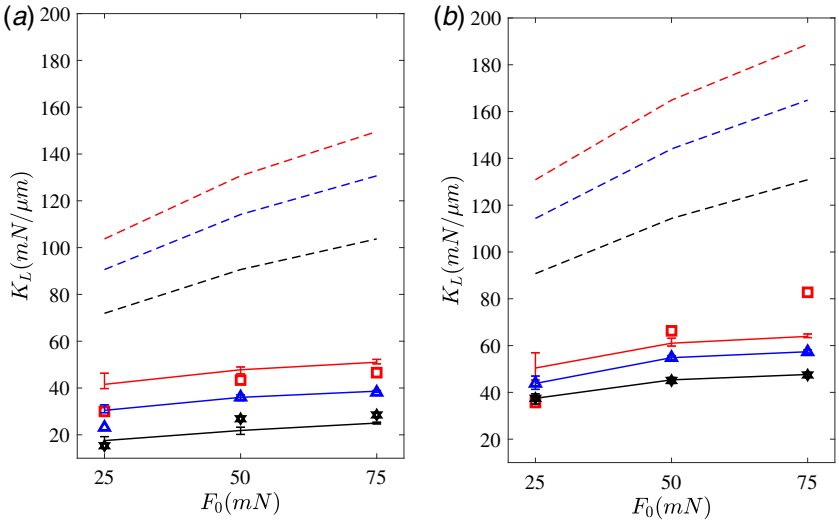

Fig. 15 Comparison between the experimental (solid lines), numerical (markers), and Mindlin (dashed lines) lateral stiffness at points A (red), B (blue), and C (black) for (*a*) HDPE and (*b*) POM contact on the silicon wafer (Color version online.)

Comparing Fig. 15(*a*) with Fig. 15(*b*) reveals that, for a fixed normal load, the lateral stiffness at the POM-silicon wafer contact interface is higher than that of the HDPE-silicon wafer contacts. Three parameters can be considered for this comparison: elastic modulus, friction coefficient, and surface roughness. Based on Eq. (12), it appears that the lateral stiffness depends on the contact radius (or equivalently the contact area), friction coefficient, and elastic modulus. It is clear that the lateral stiffness is in direct relation to the elastic modulus. Increasing the coefficient of friction can also increase lateral stiffness. Yet, this increase seems to be smaller in comparison with the other parameters. The other parameter to discuss is surface roughness. As suggested by the RMS value of the surface roughness (see Fig. 5), the HDPE ball has a rougher surface. For a similar situation, it has been shown that an increase in the interface roughness decreases the contact lateral stiffness [34]. This is also confirmed by Eq. (12), where a rougher surface leads to a lower contact area and, therefore, a lower lateral stiffness. Thus, the rougher surface of the ball is the other parameter that attributes to lower lateral stiffness in the case of HDPE. In other words, increasing the roughness level decreases the contact area and consequently, the lateral stiffness. This is also confirmed by comparing the Mindlin's lateral stiffness (for a smooth contact interface) with either experimental or numerical stiffness values of the real rough interfaces as demonstrated in Fig. 15. Therefore, the higher lateral stiffness in the case of POM is attributed to its higher elastic modulus and lower surface roughness than HDPE. Although the friction coefficient is higher in the case of HDPE, it is not higher enough to compensate for the effect of its lower elastic modulus and rougher surface.

6 Conclusions

In this paper, the pre-sliding behavior at the interface of a polymeric ball, either HDPE or POM, and a silicon wafer was studied. Friction experiments were conducted at these two interfaces for different normal loads and at several spots. Extracting the friction coefficient and stroke from the experiments and using them as two inputs to a BEM model, the same friction hysteresis loops were generated to be compared with experiments. The roughness of the polymeric ball, as an important factor in pre-sliding behavior, was also measured and put into the model. The lateral stiffness of the contact was calculated at three different points on the friction loop both experimentally and numerically to quantitatively compare the results. The numerical values of the lateral stiffness were close to experimental ones, except for the point close to the curvy corners of the friction hysteresis loops. The difference in the lateral stiffness between the HDPE and POM was attributed to the difference in the elastic modulus, their surface roughness, and friction coefficient, where the first two had a dominating effect.

Acknowledgment

This research was carried out under project number S61.1.13492 in the framework of the Partnership Program of the Materials innovation institute M2i (www.m2i.nl) and the Technology Foundation TTW (www.stw.nl), which is part of the Netherlands Organization for Scientific Research (www.nwo.nl).

Nomenclature

a = Hertzian contact radius
E = elastic modulus
R = radius of the polymeric ball
S = apparent contact stiffness
d_c = contact depth
d_{in} = indentation depth
d_s = lateral displacement stroke
x_{cs} = displacement measured by the capacitive sensor
x_{ps} = *XY*-stage displacement in *x*-direction
A_c = contact area
A_{sl} = slip area
A_{st} = stick area
E_r = reduced elastic modulus between diamond tip and polymer
E_s = effective elastic modulus
F_0 = external normal force
F_{in} = indentation load
F_x = lateral force
G_s = effective shear modulus
K_c = spring constant of the spring-slider element
K_L = contact lateral stiffness
K_s = setup lateral stiffness
S_e = corrected contact stiffness
$K_L^{Mindlin}$ = contact lateral stiffness from the analytical solution of Mindlin
c_1, c_2, n = curve-fitting parameters
$g(x, y)$ = separation profile

$h(x, y)$ = initial separation
$p(x, y)$ = pressure profile
$q_{x,y}(x, y)$ = shear stress components in x and y directions
$s_{x,y}(x, y)$ = relative displacement in x and y directions
$u_{x,y,z}(x, y)$ = deformation in x, y, and z directions
$\delta_{x,y,z}$ = rigid body displacement in x, y, and z directions
ε = geometric constant
μ_f = coefficient of friction
ν = Poisson's ratio

References

[1] Cattaneo, C., 1938, "Sul Contatto Di Due Corpi Elastici: Distribuzione Locale Degli Sforzi," Atti Accad Naz Lincei, **27**, pp. 342–348.
[2] Mindlin, R. D., 1949, "Compliance of Elastic Bodies in Contact," J. Appl. Mech., **16**, pp. 259–268.
[3] Mindlin, R. D., and Deresiewicz, H., 1953, "Elastic Spheres in Contact Under Varying Oblique Force," J. Appl. Mech., **20**, pp. 327–344.
[4] Kogut, L., and Etsion, I., 2003, "A Semi-Analytical Solution for the Sliding Inception of a Spherical Contact," J. Tribol., **125**(3), pp. 499–506.
[5] Wang, R. H., Jain, V. K., and Mall, S., 2007, "A Non-Uniform Friction Distribution Model for Partial Slip Fretting Contact," Wear, **262**(5–6), pp. 607–616.
[6] Yue, T., and Abdel Wahab, M., 2017, "Finite Element Analysis of Fretting Wear Under Variable Coefficient of Friction and Different Contact Regimes," Tribol. Int., **107**, pp. 274–282.
[7] Chen, W. W., Liu, S., and Wang, Q. J., 2008, "Fast Fourier Transform Based Numerical Methods for Elasto-Plastic Contacts of Nominally Flat Surfaces," J. Appl. Mech., **75**(1), p. 011022.
[8] Wang, Z. J., Wang, W. Z., Wang, H., Zhu, D., and Hu, Y. Z., 2010, "Partial Slip Contact Analysis on Three-Dimensional Elastic Layered Half Space," ASME J. Tribol., **132**(2), p. 021403.
[9] Wang, Z. J., Wang, W. Z., Meng, F. M., and Wang, J.-X., 2011, "Fretting Contact Analysis on Three-Dimensional Elastic Layered Half Space," ASME J. Tribol., **133**(3), p. 031401.
[10] Rodríguez-Tembleque, L., Abascal, R., and Aliabadi, M. H., 2011, "A Boundary Elements Formulation for 3D Fretting-Wear Problems," Eng. Anal. Boundary Elem., **35**(7), pp. 935–943.
[11] Gallego, L., Nélias, D., and Deyber, S., 2010, "A Fast and Efficient Contact Algorithm for Fretting Problems Applied to Fretting Modes I, II and III," Wear, **268**(1–2), pp. 208–222.
[12] Archard, J. F., 1957, "Elastic Deformation and the Laws of Friction," Proc. R. Soc. A, **243**(1233), pp. 190 LP–205.
[13] Greenwood, J. A., and Williamson, J. P. B., 1966, "Contact of Nominally Flat Surfaces," Proc. R. Soc. A, **295**(1442), pp. 300–319.
[14] Bowden, F. P., and Tabor, D., 1986, *The Friction and Lubrication of Solids*, Oxford University Press, Oxford.
[15] Eriten, M., Polycarpou, A. A., and Bergman, L. A., 2010, "Physics-Based Modeling for Partial Slip Behavior of Spherical Contacts," Int. J. Solids Struct., **47**(18–19), pp. 2554–2567.
[16] Eriten, M., Polycarpou, A. A., and Bergman, L. A., 2011, "Physics-Based Modeling for Fretting Behavior of Nominally Flat Rough Surfaces," Int. J. Solids Struct., **48**(10), pp. 1436–1450.
[17] Farhang, K., Segalman, D., and Starr, M., 2007, "Prediction of Dissipation in Joints Subject to Oscillating Force," Proceedings of ASME/STLE International Joint Tribology Conference IJTC 2007, PART A, San Diego, CA, Oct. 22–24, pp. 475–477.
[18] Al-Bender, F., and De Moerlooze, K., 2010, "On the Relationship Between Normal Load and Friction Force in Pre-Sliding Frictional Contacts. Part 1: Theoretical Analysis," Wear, **269**(3–4), pp. 174–182.
[19] De Moerlooze, K., Al-Bender, F., and Van Brussel, H., 2010, "A Generalised Asperity-Based Friction Model," Tribol. Lett., **40**(1), pp. 113–130.
[20] Eriten, M., Polycarpou, A. A., and Bergman, L. A., 2011, "Surface Roughness Effects on Energy Dissipation in Fretting Contact of Nominally Flat Surfaces," ASME J. Appl. Mech., **78**(2), 021011.
[21] Song, B., and Yan, S., 2017, "Relationship Between the Real Contact Area and Contact Force in Pre-Sliding Regime," Chin. Phys. B, **26**(7).
[22] Raeymaekers, B., and Talke, F. E., 2010, "The Effect of Laser Polishing on Fretting Wear Between a Hemisphere and a Flat Plate," Wear, **269**(5–6), pp. 416–423.
[23] Pohrt, R., and Li, Q., 2014, "Complete Boundary Element Formulation for Normal and Tangential Contact Problems," Phys. Mesomech., **17**(4), pp. 334–340.
[24] Paggi, M., Pohrt, R., and Popov, V. L., 2014, "Partial-Slip Frictional Response of Rough Surfaces," Sci. Rep., **4**(1), p. 5178.
[25] Grzemba, B., Pohrt, R., Teidelt, E., and Popov, V. L., 2014, "Maximum Micro-Slip in Tangential Contact of Randomly Rough Self-Affine Surfaces," Wear, **309**(1–2), pp. 256–258.
[26] Kasarekar, A. T., Bolander, N. W., Sadeghi, F., and Tseregounis, S., 2007, "Modeling of Fretting Wear Evolution in Rough Circular Contacts in Partial Slip," Int. J. Mech. Sci., **49**(6), pp. 690–703.
[27] Chen, S. C., Wei, P. J., and Lin, J. F., 2009, "A Model Developed for the Adhesion Forces Formed Between an Atomic Force Microscopy Tip and a Rough Surface Under Different Humidity Levels," Jpn J. Appl. Phys., **48**(5R), p. 0550011.
[28] Bazrafshan, M., de Rooij, M. B., and Schipper, D. J., 2019, "The Effect of Adhesion and Roughness on Friction Hysteresis Loops," Int. J. Mech. Sci., **155**, pp. 9–18.
[29] Bazrafshan, M., de Rooij, M. B., and Schipper, D. J., 2018, "Adhesive Force Model at a Rough Interface in the Presence of Thin Water Films: The Role of Relative Humidity," Int. J. Mech. Sci., **140**, pp. 471–485.
[30] Bazrafshan, M., de Rooij, M. B., Valefi, M., and Schipper, D. J., 2017, "Numerical Method for the Adhesive Normal Contact Analysis Based on a Dugdale Approximation," Tribol. Int., **112**, pp. 117–128.
[31] Yaqoob, M. A., de Rooij, M. B., and Schipper, D. J., 2012, "Design of a Vacuum Based Test Rig for Measuring Micro Adhesion and Friction Force," High Perform. Struct. Mater., **124**, pp. 261–274.
[32] Oliver, W. C., and Pharr, G. M., 1992, "An Improved Technique for Determining Hardness and Elastic Modulus Using Load and Displacement Sensing Indentation Experiments," J. Mater. Res., **7**(6), pp. 1564–1583.
[33] Tang, B., and Ngan, A. H. W., 2003, "Accurate Measurement of tip—Sample Contact Size During Nanoindentation of Viscoelastic Materials," J. Mater. Res., **18**(5), pp. 1141–1148.
[34] Bazrafshan, M., de Rooij, M. B., and Schipper, D. J., 2018, "On the Role of Adhesion and Roughness in Stick-Slip Transition at the Contact of two Bodies: A Numerical Study," Tribol. Int., **121**, pp. 381–388.